SUPPLEMENTAL FIGURE LEGENDS

Figure S1, Related to figure 1-2. AGO2 is nuclear in stem cells and progenitor cells. A, Satellite cell isolation by Florescence-activated cell sorting (FACS). VCAM1 positive and Pacific Blue labeled Sca1, APC labeled CD31/CD45, and Sytox Green negative cell population were sorted. **B,** AGO1-4 immunoblots in doxycycline induced and uninduced AGO1-4$^{-/-}$ whole cell lysates. GAPDH serves as loading control. Note that ab57113 recognizes an unknown nuclear antigen at ~100 kDa. **C,** AGO1-4 immunoblots in AGO2$^{-/-}$ mouse embryonic fibroblasts (MEFs). GAPDH serves as loading control. **D,** Immunofluorescence staining of doxycycline induced and uninduced AGO1-4$^{-/-}$ cells using anti-FLAG and anti-AGO2 11A9 antibody (Millipore). Dapi stains the DNA. **E,** AGO2 immunofluorescence staining in a panel of human and murine cell lines. hMB: human skeletal muscle cells, iPSC: cell line NTCR-5. Phalloidin stained for F-actin, Dapi stained for DNA and HIST3H3 stained for chromatin. **F,** Autoradiograph of a denaturing polyacrylamide gel fractionating radiolabeled RNAs recovered from FLAG-IP from whole cell lysates of AGO1-4$^{-/-}$ and AGO1-4$^{-/-}$ transiently expressing WT-AGO2, as well as cytoplasmic and nuclear AGO1-4$^{-/-}$ ESC fractions overexpressing NLS-AGO2. **G,** Schematic representation of experimental setup for Figure 2F.

Figure S2, Related to figure 3. AGO2 is loaded with mature miRNA in the nucleus. A, Immunoblot for FLAG-AGO2 controlling for IP with Pan-AGO affinity peptide-IP (WT) and Control (Ctrl.) peptides in cytoplasmic and nuclear fractionation from 2 day differentiated myocytes. **B,** Autoradiograph of a denaturing polyacrylamide gel fractionating radiolabeled RNAs recovered from Pan-AGO affinity peptide-IP (WT) and Control (Ctrl.) peptides from the cytoplasmic and nuclear fractions of 2 day differentiated myocyte lysates. The lower panel shows immunoblots for FLAG-AGO2 controlling for IP. **C**, Scatterplot comparing the cytoplasmic and the nuclear miRNA profiles from 2 day differentiated myocytes.

Figure S3, Related to figure 4. Nuclear AGO2 binds thousands of different mRNAs target. **A,** Autoradiograph of crosslinked and radiolabeled Pan-AGO affinity peptide-IP ribonucleoprotein separated by SDS-PAGE. The lower panel shows immunoblots for FLAG-AGO2 controlling for IP, as well as CALR and LMNA controlling for cellular fractionations. **B,** Distribution of PAR-CLIP sequence reads across target mRNA 3'UTR, coding sequence, 5'UTR, and introns. **C,** Cumulative distribution function of the conservation score of AGO2 intronic binding sites (red line) compared to a cohort of five expression matched (blue line, left panel) or a cohort of five expression and di-nucleotide composition matched (blue line, right panel) background sets of random intronic sequences. The table indicates details for each cohort of background sets, including p-values calculated by Mann-Whitney U-test compared to intronic PAR-CLIP sites. **D,** Enrichment of seed complementary sequence for the top 9 most abundant miRNAs in AGO1-4$^{-/-}$-FHAGO2 cells across target mRNA clusters in 3'UTR, coding and intronic sequence in

cytoplasmic (top) and nuclear (bottom) PAR-CLIP binding sites. Position 0 indicates the predominant T-to-C transition in target mRNA clusters.

Figure S4, Related to figure 5. AGO2 destabilizes RNA targets in the nucleoplasm. A, mRNA expression changes upon AGO2 induction in AGO1-4$^{-/-}$-FHAGO2 ESCs determined by RNAseq from total fraction. The cumulative distribution of cytoplasmic AGO2 PAR-CLIP targets binned by number of binding sites compared non-AGO2 targets. *P*-values are determined by Mann-Whitney U-test. **B,** mRNA expression changes upon AGO2 induction in AGO1-4$^{-/-}$-FHAGO2 ESCs determined by RNAseq from nuclear fraction. The cumulative distribution of nuclear AGO2 PAR-CLIP targets binned by number of binding sites compared non-AGO2 targets. *P*-values are determined by Mann-Whitney U-test. **C,** Cumulative distribution of abundance changes in RNA extracted from the chromatin fraction upon AGO2 induction in AGO1-4$^{-/-}$-FHAGO2 ESCs determined by RNAseq. Nuclear AGO2 PAR-CLIP targets binned by number of binding sites compared non-AGO2 targets. *P*-values were determined by Mann-Whitney U-test. **D,** Cumulative distribution of abundance changes in cytoplasmic RNA upon AGO2 induction in AGO1-4$^{-/-}$-FHAGO2 ESCs determined by RNAseq. Nuclear AGO2 PAR-CLIP targets were binned by the presence of binding sites exclusively in the 3'UTR, CDS, or intron and compared to non-targets. *P*-values were determined by Mann-Whitney U-test. **E,** AGO2 immunoblots from cytoplasmic and nuclear lysates after miR-16 transfection. The endoplasmic reticulum protein CALR served as cytoplasmic marker and LMNA served as nuclear markers. **F,** Relative read frequency of before and after miR-16 transfection determined by small RNA sequencing. **G,** Cumulative distribution of abundance changes in cytoplasmic RNA upon miR-16 introduction into AGO1-4$^{-/-}$-FHAGO2 ESCs. Experimentally determined miR-16 target sites were downloaded from miRdb.org and binned according to binding in 3'UTR and CDS.

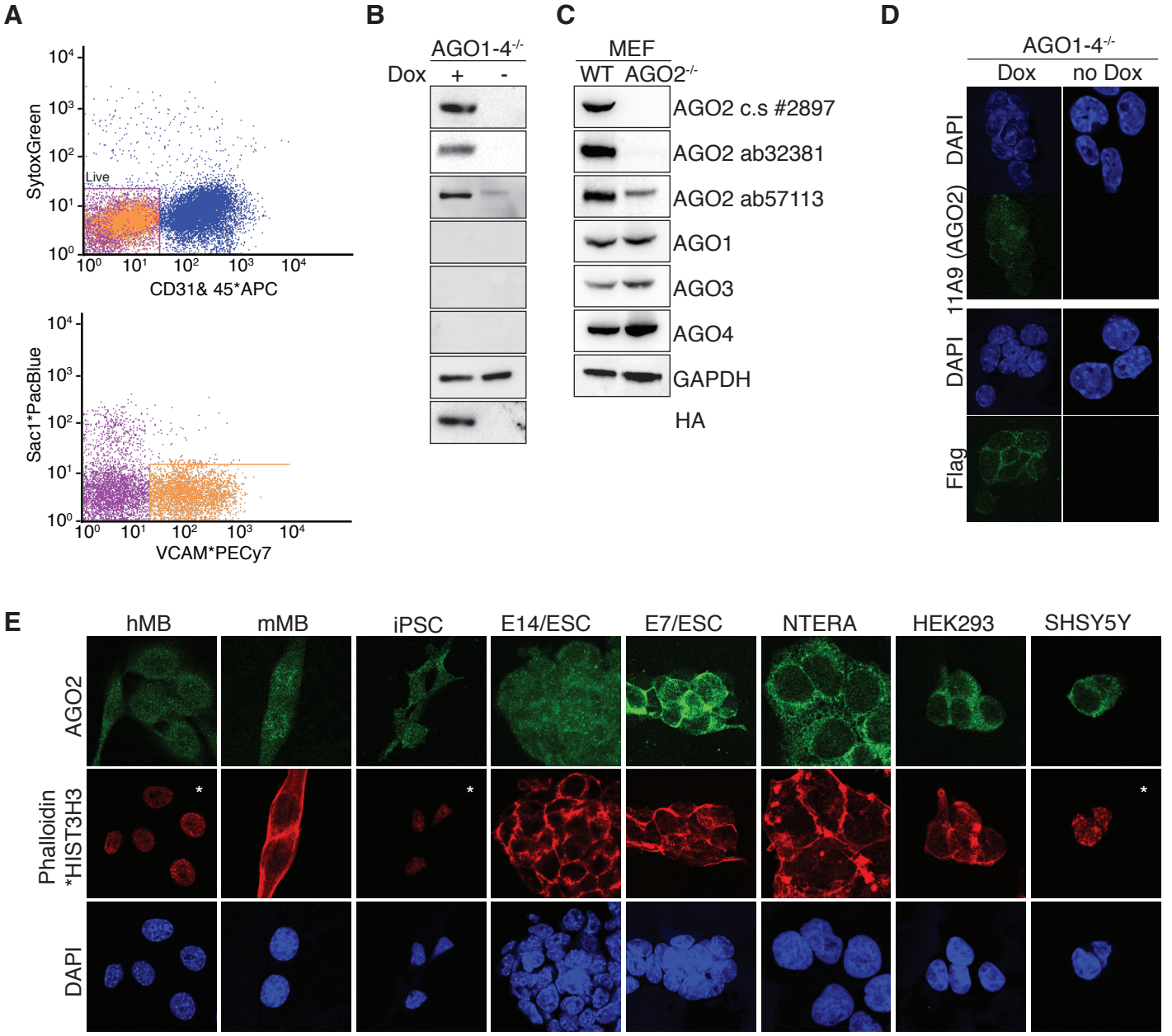

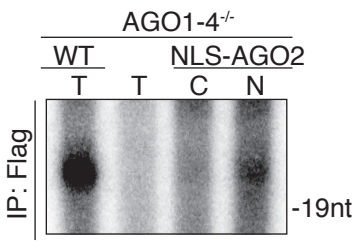

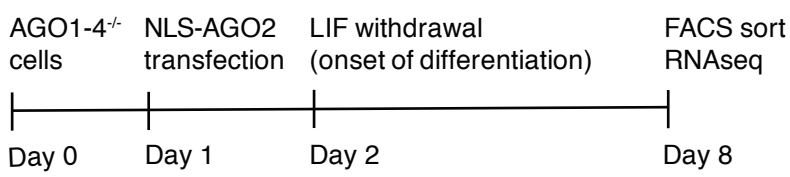

Sarshad et al. Fig S1

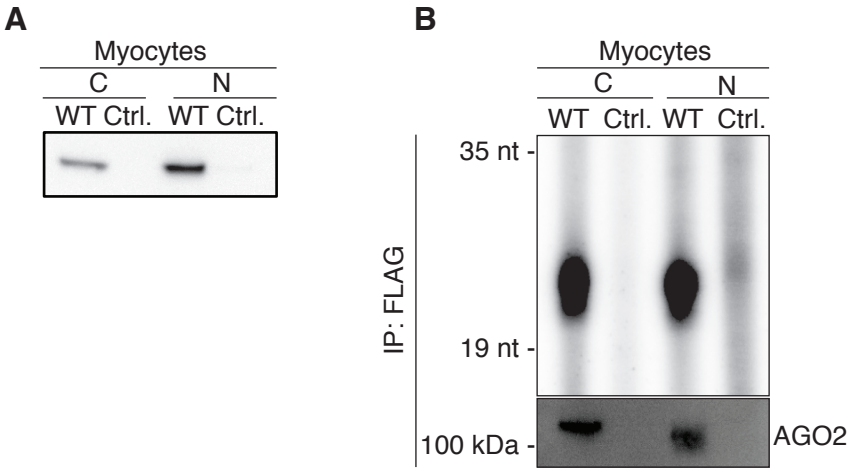

Sarshad et al. Fig S2

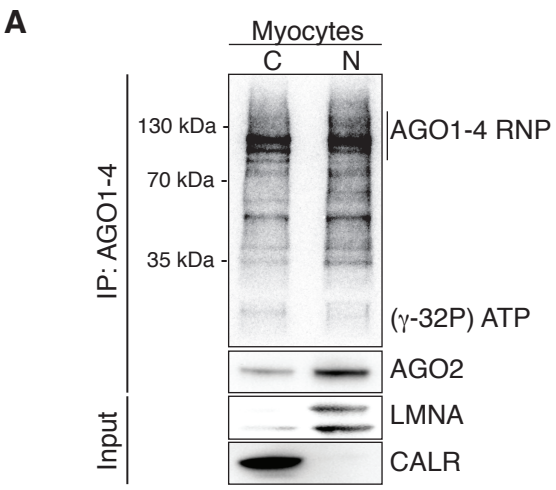

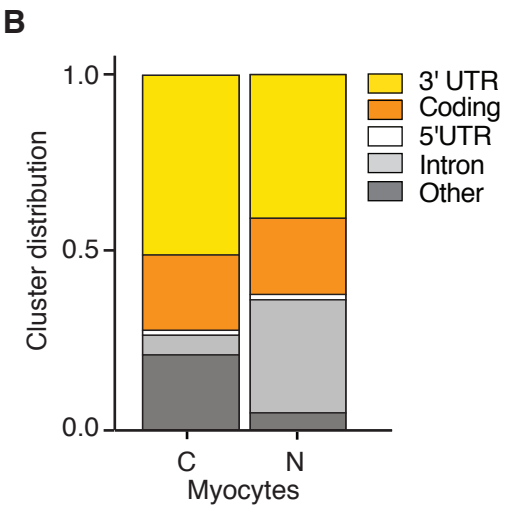

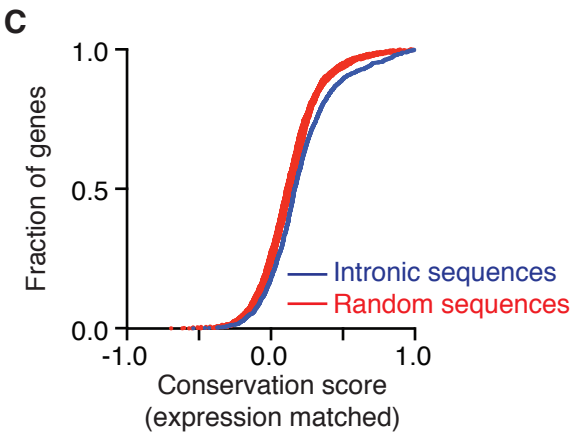

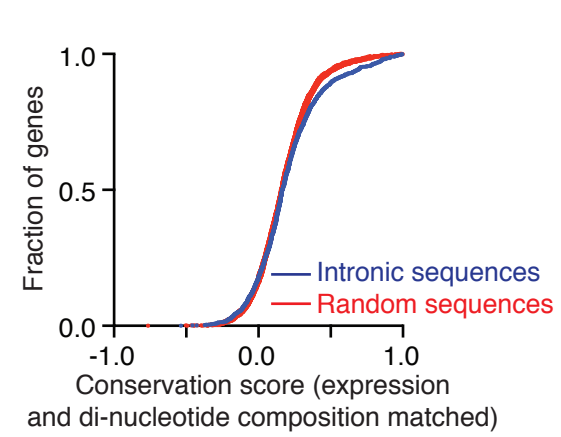

	Sequences	Lifted to hg38	Mean conservation score	p-value against random sequence set
Source of random seqs	**Intron binding sites**	**1459**	**0.203**	**---**
Expression matched	Random set 1	1117	0.147	1.75E-07
	Random set 2	1180	0.127	3.39E-16
	Random set 3	1164	0.133	1.24E-14
	Random set 4	1131	0.135	4.84E-13
	Random set 5	1177	0.131	2.97E-14
Expression and di-nucleotide composition matched	Random set 1	1372	0.176	0.049
	Random set 2	1399	0.177	0.034
	Random set 3	1335	0.176	0.026
	Random set 4	1387	0.179	0.077
	Random set 5	1363	0.178	0.035

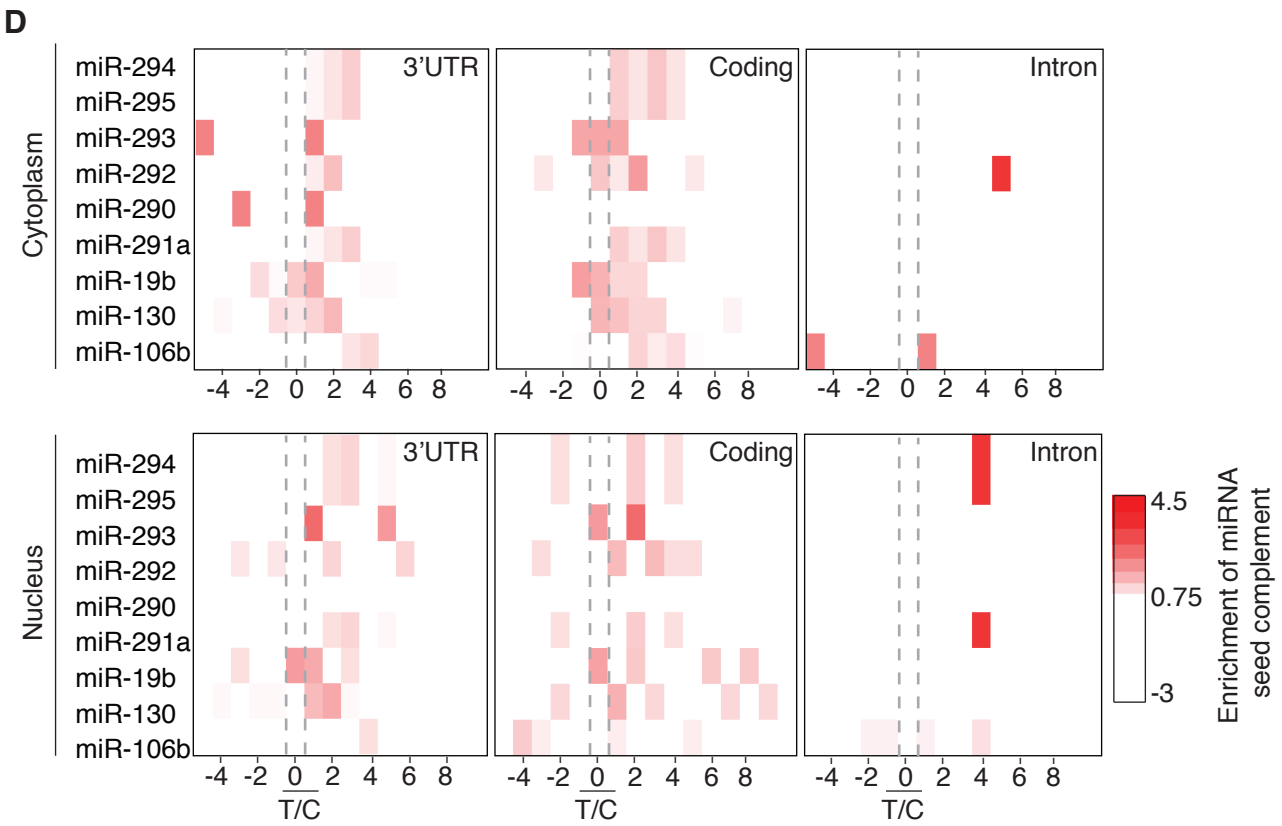

Sarshad et al. Fig S3

A

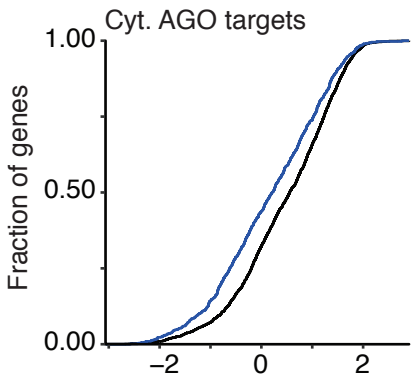

mRNA abundance change [log_2Total RNA AGO1-4$^{-/-}$-FHAGO2 / AGO1-4$^{-/-}$]

Cytoplasmic targets n = 837 p = 6.27E-13
No target n = 2307

B

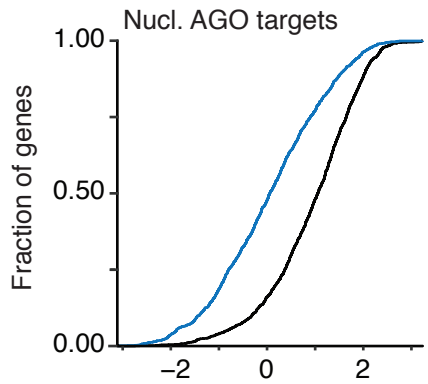

mRNA abundance change [log_2 Nucl. RNA AGO1-4$^{-/-}$-FHAGO2 / AGO1-4$^{-/-}$]

Nuclear target n = 1167 p = 1.90E-80
No target n = 1241

C

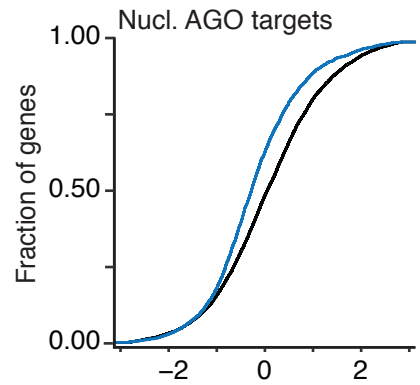

mRNA abundance change [log_2 Chr. RNA AGO1-4$^{-/-}$-FHAGO2 / AGO1-4$^{-/-}$]

Chromatin targets n = 2746 p = 2E-16
No target n = 8536

D

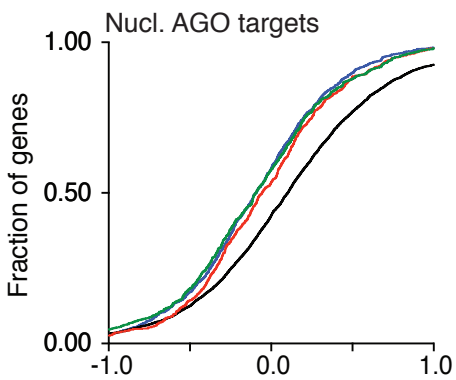

mRNA abundance change [log_2 Cyt.RNA AGO1-4$^{-/-}$-FHAGO2 / AGO1-4$^{-/-}$]

Intron n = 674 p = 1.31E-29
3'UTR n = 869 p = 1.3E-21
Coding n = 332 p = 3.9E-10
No target n = 5179

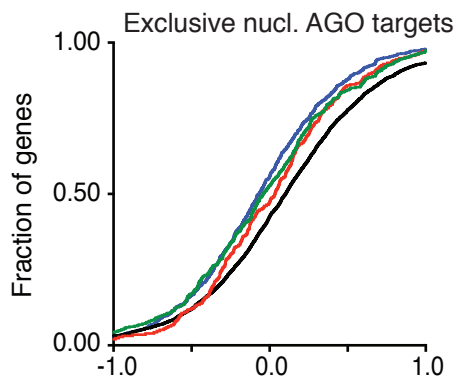

mRNA abundance change [log_2 Cyt.RNA AGO1-4$^{-/-}$-FHAGO2 / AGO1-4$^{-/-}$]

Intron n = 726 p = 4.96E-14
3'UTR n = 421 p = 2.55E-04
Coding n = 254 p = 1.78E-02
No target n = 4223

E

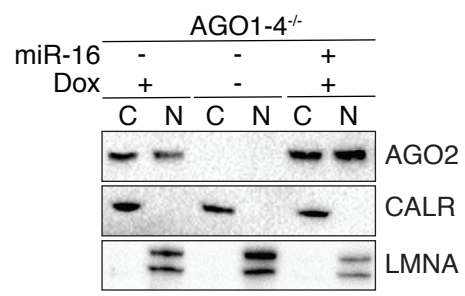

F

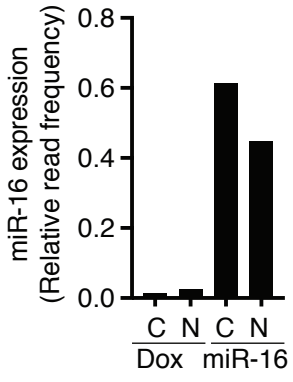

G

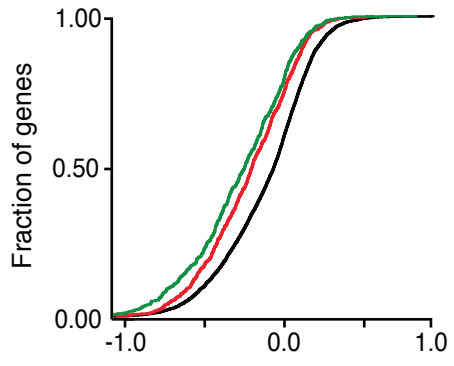

mRNA abundance change [log_2 Cyt.RNA AGO1-4$^{-/-}$-FHAGO2 / AGO1-4$^{-/-}$-FHAGO2-miR-16]

Coding n = 987 p = 6.53E-16
3'UTR n = 437 p = 6.53E-28
No target n = 6392